

# 1 **Broadband Nonreciprocal Thermal Emission**

2 Zhenong Zhang<sup>1</sup> and Linxiao Zhu<sup>\*,1</sup>

3 <sup>1</sup> Department of Mechanical Engineering, The Pennsylvania State University, University Park,  
4 PA 16802, United States

5 <sup>\*</sup>Corresponding email: [lqz5242@psu.edu](mailto:lqz5242@psu.edu)

## 8 **Abstract**

9 The reciprocity between thermal emission and absorption in materials that satisfy the  
10 Lorentz reciprocity places a fundamental constraint on photonic energy conversion and thermal  
11 management. For approaching the ultimate thermodynamic limits in various photonic energy  
12 conversion and achieving nonreciprocal radiative thermal management, broadband nonreciprocal  
13 thermal emission is desired. However, existing designs of nonreciprocal emitters are narrow-  
14 banded. Here, we introduce gradient epsilon-near-zero magneto-optical metamaterial for achieving  
15 broadband nonreciprocal thermal emission. We start by analyzing the nonreciprocal thermal  
16 emission and absorption in a thin layer of epsilon-near-zero magneto-optical material atop a  
17 substrate. We use temporal coupled mode theory to elucidate the mechanism of nonreciprocal  
18 emission in the thin film emitter. We then introduce a general approach for achieving broadband  
19 nonreciprocal emission by using a gradient epsilon-near-zero magneto-optical metamaterial. We  
20 numerically demonstrate broadband nonreciprocal emission in gradient-doped semiconductor  
21 multilayer, as well as in a magnetic Weyl semimetal multilayer with gradient chemical potential.  
22 Our approach for achieving broadband nonreciprocal emitters will be useful for developing  
23 broadband nonreciprocal devices for energy conversion and thermal management.

1      **I. Introduction**

2              Controlling thermal emission and absorption is important for applications [1-4] in energy  
3      conversion, thermal management, lighting, and imaging. Various photonic structures and materials  
4      have been used to control emission and absorption, such as metamaterials [5, 6], metasurfaces [7,  
5      8], photonic crystals [9-11], multilayer [12, 13], epsilon-near-zero materials [14, 15], two-  
6      dimensional materials [16, 17], and phase-change materials [18], leading to applications such as  
7      thermophotovoltaics [19-21], solar cells [22, 23], and radiative cooling [12, 24]. However, the  
8      emission and absorption processes are typically constrained by a reciprocity relation. The  
9      Kirchhoff's law of thermal radiation [25-27] states that the emissivity equals the absorptivity at  
10     the same angle and frequency. Such reciprocity between emission and absorption places a stringent  
11     constraint on the performance of a range of applications such as solar cells [28-30],  
12     thermophotovoltaics [31], and harvesting outgoing radiation [31, 32].

13              Achieving nonreciprocal emission and absorption points to a fundamental pathway for  
14     improving a range of energy harvesting technologies, such as solar energy harvesting [28-30],  
15     thermophotovoltaics [31], harvesting energy from outgoing radiation [31], and simultaneously  
16     harvesting energy from the sun and the outer space [32]. Importantly, to achieve the ultimate  
17     thermodynamic limits in these applications [28-32], nonreciprocal emission and absorption all  
18     need be achieved over a broad band. A reciprocal solar cell needs emit luminescence towards the  
19     sun. Such luminescence cannot be used, and it represents energy loss. In contrast, a nonreciprocal  
20     solar cell can emit luminescence towards a direction away from the sun. Such luminescence can  
21     be collected using additional solar cells, leading to improvement of the overall efficiency. It has  
22     been pointed out that by using an array of nonreciprocal multijunction solar cells [29], or a  
23     nonreciprocal semitransparent multijunction solar cell [30], which achieve nonreciprocal emission

1 over all wavelengths, the efficiency can approach the Landsberg limit of 93.3%. Such efficiency  
2 is substantially higher than the limit of 86.8% in reciprocal systems. For thermophotovoltaics, the  
3 use of nonreciprocal emitters points to the possibility of achieving Carnot efficiency limit with  
4 maximum power output, which is impossible with reciprocal systems [31]. We also note that by  
5 using narrowband nonreciprocal emitters in thermophotovoltaics, it is possible to achieve Carnot  
6 efficiency limit, but with reduced power output. Further, broadband nonreciprocal emitters point  
7 to great potential for improving harvesting energy from outgoing thermal radiation. For harvesting  
8 thermal radiation from an ambient at 300 K to the outer space at 3 K, with nonreciprocal systems,  
9 the operating power density can approach a Landsberg limit [31] at  $153.1 \text{ W m}^{-2}$ , which greatly  
10 exceeds the limit of  $55 \text{ W m}^{-2}$  in reciprocal systems [31]. Also, broadband nonreciprocal emitters  
11 point to improving co-harvesting energy from the sun and the outer space [32].

12 Besides energy harvesting, achieving nonreciprocal emission and absorption points to  
13 nonreciprocal heat flux control [33] and communication [34]. For nonreciprocal heat flux control  
14 and communication, broadband nonreciprocal emitters are desirable for enhancing the magnitude  
15 of heat flux, and bandwidth of communication, respectively.

16 Nonreciprocal emission and absorption have been predicted in systems with magneto-  
17 optical materials [35-38], Kerr nonlinearity [39] or time-modulation [40]. Existing designs of  
18 nonreciprocal emitters typically rely on critical coupling in one resonance [35-37] or two  
19 resonances [41, 42]. Accordingly, strong nonreciprocal emission is achieved only near one or two  
20 resonances, leading to narrow bandwidth. To date, despite the importance of broadband  
21 nonreciprocal emission for energy harvesting, heat flux control, and communication, a general  
22 strategy for achieving broadband nonreciprocal emission is elusive.

1 In this article, we introduce a general approach for achieving broadband nonreciprocal  
 2 emission by using gradient epsilon-near-zero magneto-optical metamaterial. We elucidate the  
 3 mechanism of nonreciprocal emission in a thin film using a temporal coupled mode theory. We  
 4 then numerically demonstrate broadband nonreciprocal emission in gradient doped  
 5 semiconductors, and magnetic Weyl semimetals with gradient chemical potential. Our results can  
 6 be useful for developing broadband nonreciprocal devices for energy conversion and thermal  
 7 management.

8 **II. Nonreciprocal emission in a single magneto-optical layer**

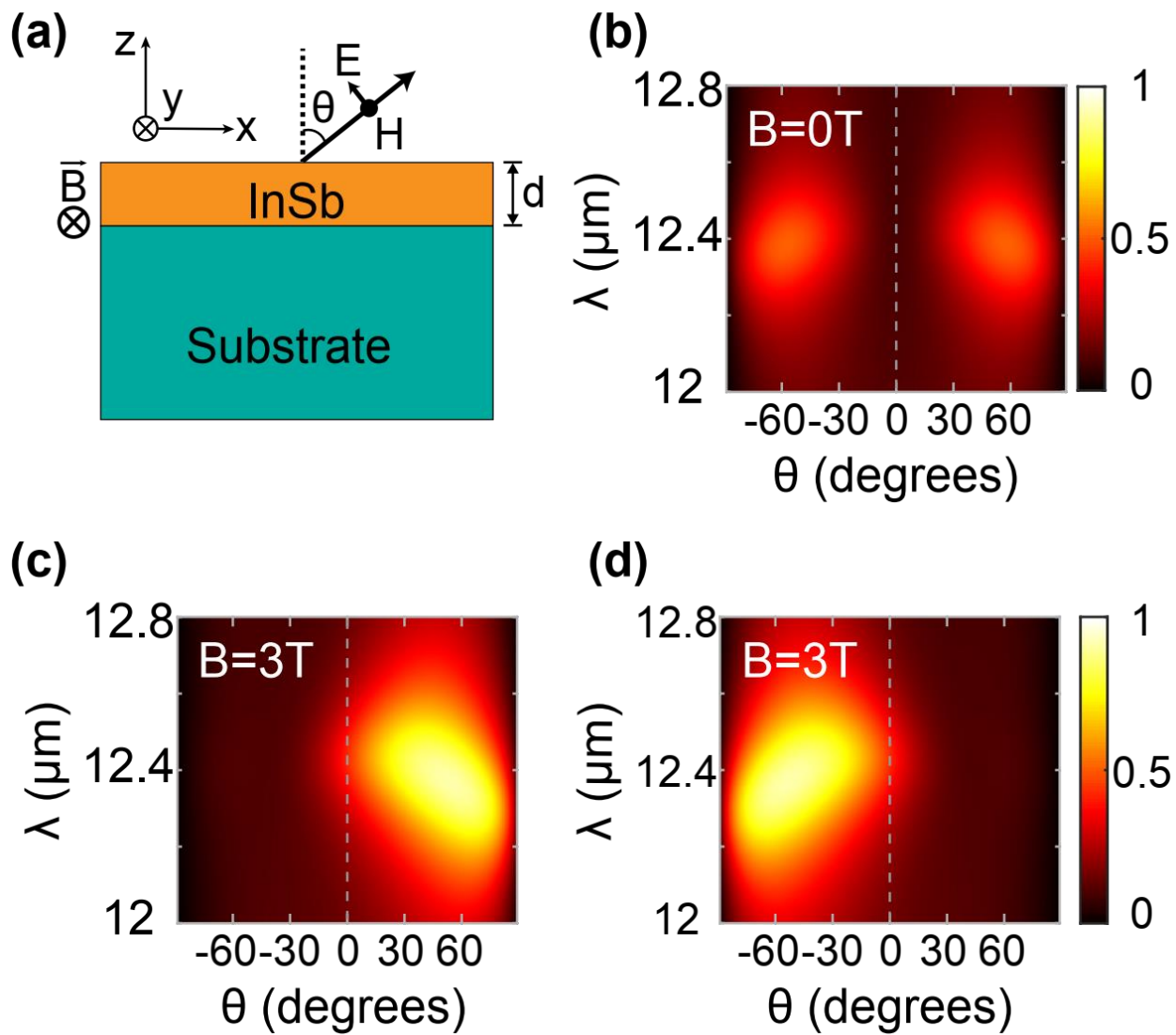
9 We begin by considering emission and absorption in a thin film emitter shown in Fig. 1(a).  
 10 The emitter consists of a magneto-optical film on top of a substrate. Without loss of generality, we  
 11 consider 400 nm thick doped InSb film, and a substrate with relative permittivity  $\epsilon_s = -2$ . We  
 12 consider TM polarization with emission angle  $\theta$ . We first introduce the dielectric model of doped  
 13 semiconductor. For doped semiconductor, in external magnetic field, due to free-carrier effect, the  
 14 permittivity of the material is described by a nonsymmetric tensor [43]. With magnetic field along  
 15 the  $y$  axis, the relative permittivity tensor of doped InSb is:

$$16 \quad \vec{\epsilon} = \begin{bmatrix} \epsilon_\infty - \frac{\omega_p^2(\omega - i\Gamma)}{\omega[(\omega - i\Gamma)^2 - \omega_c^2]} & 0 & -\frac{i\omega_p^2\omega_c}{\omega[(\omega - i\Gamma)^2 - \omega_c^2]} \\ 0 & \epsilon_\infty - \frac{\omega_p^2}{\omega(\omega - i\Gamma)} & 0 \\ \frac{i\omega_p^2\omega_c}{\omega[(\omega - i\Gamma)^2 - \omega_c^2]} & 0 & \epsilon_\infty - \frac{\omega_p^2(\omega - i\Gamma)}{\omega[(\omega - i\Gamma)^2 - \omega_c^2]} \end{bmatrix},$$

17 where  $\epsilon_\infty = 15.68$  is the high-frequency permittivity,  $\omega_p = \sqrt{n_e e^2 / (m^* \epsilon_0)}$  is the plasma  
 18 frequency,  $\Gamma$  is the relaxation rate, and  $\omega_c = eB/m^*$  is the cyclotron frequency. Here,  $n_e$  is the  
 19 electron doping concentration,  $e$  is the charge for a proton,  $m^*$  is the effective electron mass, and  
 20  $\epsilon_0$  is the vacuum permittivity. We consider a doping concentration  $n_e = 8 \times 10^{18} \text{ cm}^{-3}$ . At such

1 doping concentration, the electron mobility is  $\mu_n = 6730 \text{ cm}^2 \text{ V}^{-1} \text{ s}^{-1}$  [44],  $m^* = 0.707 m_e$   
 2 where  $m_e$  is the rest mass of the electron, and the relaxation rate  $\Gamma = 3.658 \times 10^{12} \text{ rad s}^{-1}$  from  
 3  $\mu_n = e/(m^* \Gamma)$ . The effective electron mass is calculated using a model [45, 46] considering the  
 4 nonparabolicity of the conduction band  $m^* = m_n \left[ 1 + \frac{1}{2} \left( \frac{3}{\pi} \right)^{\frac{2}{3}} \frac{h^2}{E_g m_n} n_e^{\frac{2}{3}} \right]^{1/2}$ , where the bandgap  
 5 energy is  $E_g = 0.17 \text{ eV}$  at 300 K,  $m_n = 0.014 m_e$  is the electron effective mass at the bottom of  
 6 the conduction band, and  $h$  is the Planck's constant.

7



8

1 FIG. 1. Nonreciprocal emitter based on one layer of magneto-optical material. (a) Schematic of a  
2 doped InSb layer on top of a substrate. The InSb layer has a thickness of  $400\text{ nm}$ , and is doped  
3 with electron concentration of  $8 \times 10^{18}\text{ cm}^{-3}$ . The substrate has constant relative permittivity  
4  $\epsilon_s = -2$ . (b) The calculated emissivity  $\epsilon$  and absorptivity  $\alpha$  of the structure in (a) as a function of  
5 wavelength and angle when there is no external magnetic field. Here, the emissivity and  
6 absorptivity are identical. (c) Calculated emissivity  $\epsilon$  and (d) absorptivity  $\alpha$  of the structure in (a)  
7 under a  $3\text{ T}$  magnetic field. The emissivities in (b-c) are calculated using fluctuational  
8 electrodynamics.

9 We calculate the emissivity and absorptivity of the structure in Fig. 1(a) using fluctuational  
10 electrodynamics [35, 47, 48]. Without external magnetic field, the emissivity and absorptivity are  
11 reciprocal, i.e.,  $\epsilon(\theta, \lambda) = \alpha(\theta, \lambda)$ , as shown in Fig. 1(b). In such case, due to the mirror symmetry  
12 with respect to the  $y$ - $z$  plane, the emissivity is symmetric with respect to angle  $\theta$ , that is  $\epsilon(\theta, \lambda) =$   
13  $\epsilon(-\theta, \lambda)$ . The emission and absorption are due to Berreman mode [14] at wavelength about  
14  $12.4\text{ }\mu\text{m}$ , where the diagonal component of permittivity ( $\epsilon_{xx}$ ) of the magneto-optical layer is near  
15 zero (Fig. 3(b)).

16 With an external magnetic field applied along the  $y$  axis, the emissivity and absorptivity  
17 change in opposite trends, as shown in Fig. 1(c-d). With  $3\text{ T}$  magnetic field, compared with the  
18 case without magnetic field, the emissivity is greatly enhanced at angle  $\theta > 0$  (Fig. 1(c)), and the  
19 absorptivity is greatly suppressed at angle  $\theta > 0$  (Fig. 1(d)). The enhancement of emissivity and  
20 the suppression of absorptivity at the same angle lead to strong breaking of the Kirchhoff's law of  
21 thermal radiation, i.e.,  $\epsilon(\theta, \lambda) \neq \alpha(\theta, \lambda)$ . As an example, at angle  $\theta = 60^\circ$  and wavelength  $\lambda =$   
22  $12.35\text{ }\mu\text{m}$ , the emissivity and absorptivity are 0.908 and 0.112, respectively.

### 23 **III. Temporal coupled mode theory**

24 We employ temporal coupled mode theory to elucidate the mechanism of the strong  
25 nonreciprocal emission [49]. We consider an emission mode at resonance frequency  $\omega_r$ . From  
26 temporal coupled mode theory, the emissivity is

$$\varepsilon = \frac{4\gamma_i\gamma_e}{(\omega - \omega_r)^2 + (\gamma_i + \gamma_e)^2}, \quad (1)$$

1 where  $\omega$  is the angular frequency. For the emission mode, the total modal decay rate is the sum of  
 2 an intrinsic decay rate  $\gamma_i$  due to material loss and an external decay rate  $\gamma_e$  due to radiation. For a  
 3 nearly lossless version of the emission mode, that is, when the intrinsic decay rate is near zero, the  
 4 external decay rate exclusively defines the total modal decay rate.

5 We solve the dispersion relation for the thin film emitter structure shown in Fig. 1(a), for  
 6 both the lossy case, and the nearly lossless case with  $\Gamma$  set to zero. The dispersion relation  $\omega(k_x)$  of  
 7 the TM mode for the thin film structure [50] is given by:

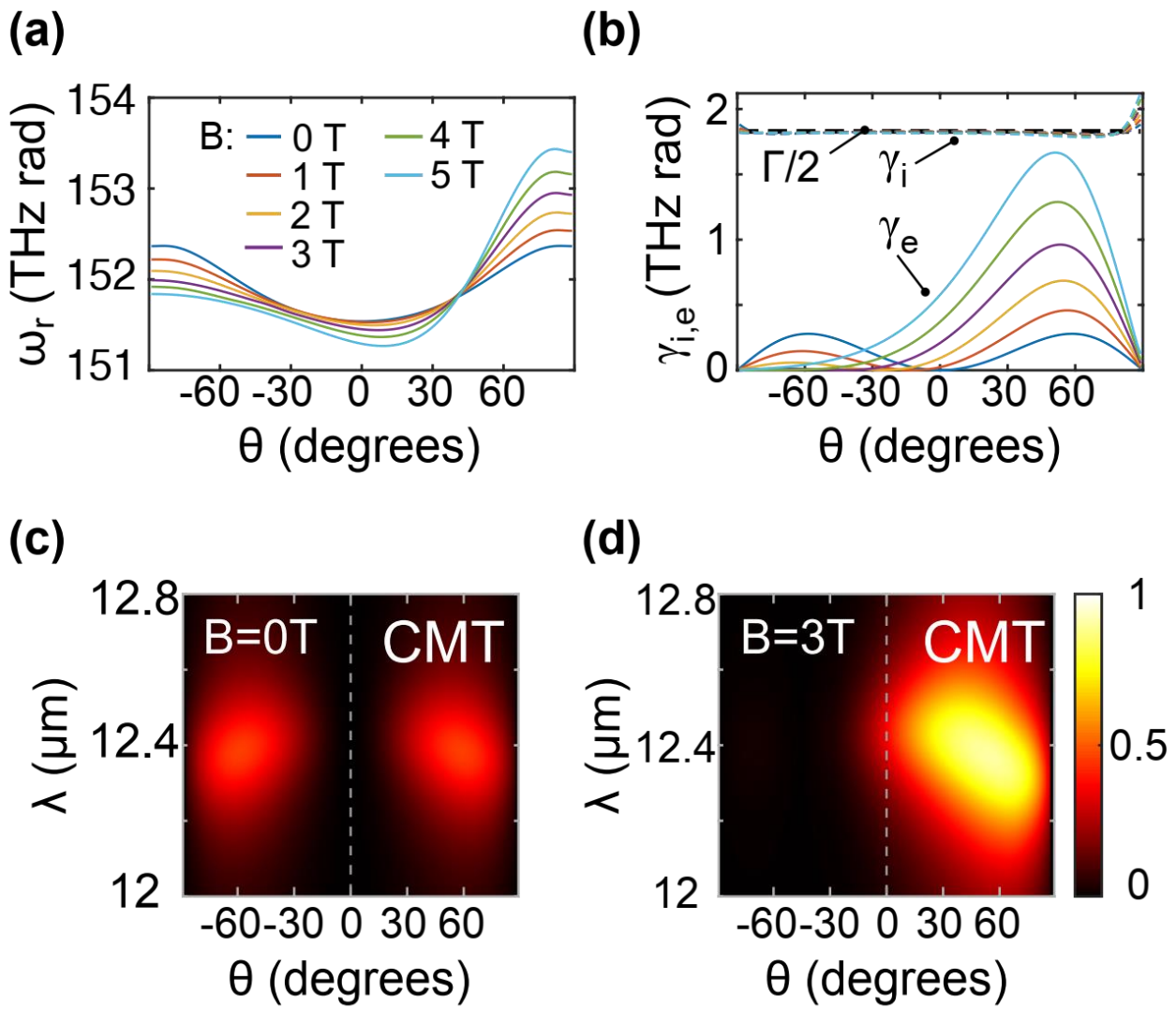
$$i\tan(k_z d) = -\frac{\epsilon_{xx}k_z \left(k_{z,V} + \frac{k_{z,S}}{\epsilon_S}\right)}{\epsilon_{xx}k_0^2 - k_x^2 + k_x\epsilon_{xz} \left(k_{z,V} - \frac{k_{z,S}}{\epsilon_S}\right) + k_{z,V} \frac{k_{z,S}(\epsilon_{xx}^2 + \epsilon_{xz}^2)}{\epsilon_S}}. \quad (2)$$

8 Here,  $k_x$  is the wavevector along  $x$  axis,  $k_0 = \omega/c$  is the wavevector in vacuum where  $c$  is the  
 9 velocity of light in vacuum, and  $k_z = \sqrt{k_0^2 \left(\epsilon_{xx} + \frac{\epsilon_{xz}^2}{\epsilon_{xx}}\right) - k_x^2}$ ,  $k_{z,V} = \sqrt{k_0^2 - k_x^2}$ , and  $k_{z,S} =$   
 10  $\sqrt{\epsilon_S k_0^2 - k_x^2}$  denote the  $z$ -component of wavevector in the magneto-optical layer, vacuum, and the  
 11 substrate, respectively. As the mode has loss, we solve the dispersion relation with complex  $\omega$  and  
 12 real  $k_x$  [14]. The real part of the eigenfrequency represents the resonance frequency  $\omega_r$ , and the  
 13 imaginary part of the eigenfrequency represents the total modal loss rate. Thus, the imaginary part  
 14 of the eigenfrequency in the lossy case is  $(\gamma_i + \gamma_e)$ , and the imaginary part of the eigenfrequency  
 15 in the nearly lossless case is the external decay rate  $\gamma_e$ , from which the intrinsic decay rate  $\gamma_i$  can  
 16 be obtained as the difference between the two.

17 Figure 2(a) shows the dispersion relation of the thin film emitter at varying magnetic fields.  
 18 When there is no external magnetic field, the dispersion relation is symmetric with respect to angle

1  $\theta$ . In contrast, with external magnetic field, the dispersion relation becomes asymmetric with  
 2 respect to  $\theta$  and thus  $k_x$ . This can be understood from the fact that with external magnetic field,  
 3 Eq. 2 has dependence on  $k_x$  in the first order via  $k_x \epsilon_{xz} \left( k_{z,V} - \frac{k_{z,S}}{\epsilon_S} \right)$ . The intrinsic decay rate as  
 4 shown in Fig. 2(b) shows negligible dependence on the magnetic field and angle. The intrinsic  
 5 decay rate is about  $\Gamma/2$ , which is consistent with fact that  $\Gamma/2$  is the upper bound for intrinsic  
 6 decay rate [51] due to material loss.

7



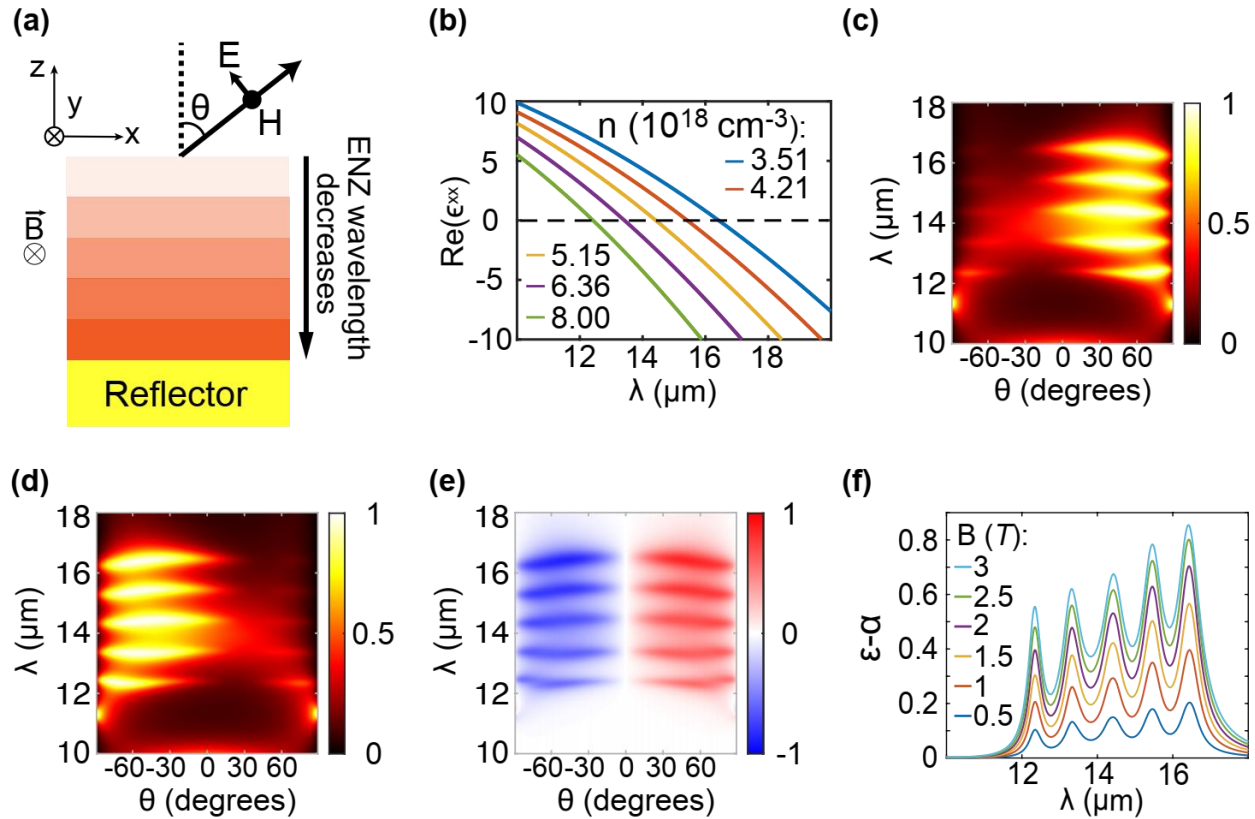
8

1 FIG. 2. Mechanism of nonreciprocal emission and absorption in one magneto-optical layer atop  
2 substrate. (a) Resonance frequency for the emission mode of the structure in Fig. 1(a) at varying  
3 angles  $\theta$  and external magnetic fields  $B$ . (b) The intrinsic decay rate (dashed lines) and external  
4 decay rate (solid lines) of the emitter at varying angles and magnetic fields. (a) and (b) share the  
5 same color labeling. The black dashed line denotes  $\Gamma/2$ , where  $\Gamma$  is the relaxation rate. (c-d)  
6 Emissivity  $\varepsilon$  predicted by temporal coupled mode theory (CMT) when (c) there is no magnetic  
7 field and (d) when there is 3 T magnetic field. The coupled mode theory uses resonance frequency  
8 in (a) and decay rates in (b).  
9

10 In contrast, the external decay rate has strong dependence on the magnetic field. As shown  
11 by Fig. 2(b), without magnetic field, the external decay rate is much smaller than the intrinsic  
12 decay rate, leading to weak emissivity. As the magnetic field increases, at  $\theta > 0$ , the external decay  
13 rate increases, leading to its improved matching with the intrinsic decay rate. Due to the better  
14 matching between the two decay rates, enhanced emissivity is expected, which is consistent with  
15 Fig. 1(c). On the other hand, as the magnetic field increases, at  $\theta < 0$ , the contrast between the  
16 two decay rates further increases, suppressing the emissivity (Fig. 1(c)). Figure 2 (c-d) show the  
17 emissivity predicted using Eq. 1 from temporal coupled mode theory, with  $\omega_r$ ,  $\gamma_i$ , and  $\gamma_e$   
18 calculated from the dispersion relations without fitting parameters. The coupled mode theory  
19 results show excellent agreement with calculation based on fluctuational electrodynamics.  
20 Therefore, the opposite changes of the external decay rates at  $\theta > 0$  and  $\theta < 0$  in response to the  
21 magnetic field lead to strong asymmetry in emissivity profile with respect to  $\theta$  under magnetic  
22 field, i.e.,  $\varepsilon(\omega, \theta) \neq \varepsilon(\omega, -\theta)$ . Moreover, as  $\alpha(\omega, \theta) = \varepsilon(\omega, -\theta)$  in specular emitters [35, 52],  
23 such asymmetry in emissivity with respect to  $\theta$  directly requires breaking of the Kirchhoff's law  
24 of thermal radiation, i.e.,  $\alpha(\omega, \theta) \neq \varepsilon(\omega, \theta)$ . It is noteworthy that when the magnetic field is  
25 sufficiently high, which is about 3 T in this case, raising the magnetic field further leads to an  
26 increase of external decay rate at all angles, indicating the existence of an optimal magnetic field  
27 for breaking the reciprocity between emissivity and absorptivity.

1 **IV. Broadband nonreciprocal emission in gradient epsilon-near-zero magneto-optical**  
 2 **metamaterial**

3 Building upon the thin film emitter, we now introduce a general approach for achieving  
 4 broadband nonreciprocal emission by using gradient epsilon-near-zero (ENZ) magneto-optical  
 5 metamaterial. The structure consists of magneto-optical multilayer on top of a reflector, as shown  
 6 in Fig. 3(a). In the multilayer, the ENZ condition for the magneto-optical material is met at  
 7 progressively shorter wavelength as the depth increases. In such way, as shown by Fig. 3(b), when  
 8 the permittivity of one magneto-optical layer reaches near zero, the magneto-optical layer  
 9 immediately underneath it has a negative permittivity, corresponding to the case of one magneto-  
 10 optical layer (Fig. 1). Nonreciprocal emission due to Berreman mode of each magneto-optical  
 11 layer can then lead to a broadband nonreciprocal emission.



1 FIG. 3. Broadband nonreciprocal emitter based on gradient epsilon-near-zero magneto-optical  
2 metamaterial. (a) Schematic of a gradient epsilon-near-zero magneto-optical metamaterial, on top  
3 of a reflector, where the ENZ wavelength of magneto-optical layer decreases with depth. (b) The  
4 real part of permittivity ( $\epsilon_{xx}$ ) of doped InSb as a function of wavelength for varying doping levels,  
5 at a magnetic field of 3 T. In (c-d), we consider gradient-doped InSb multilayer, where the doping  
6 level increases with depth. Each doped InSb layer is 400 nm thick, with the corresponding doping  
7 level shown in (b). The reflector consists of 500 nm-thick undoped InSb atop Au. (c) Emissivity  $\epsilon$ ,  
8 (d) absorptivity  $\alpha$ , and (e) difference between emissivity and absorptivity ( $\epsilon - \alpha$ ) of the gradient-  
9 doped InSb multilayer under 3 T magnetic field. (f) Difference between emissivity and absorptivity  
10 of the multilayer at  $\theta = 50^\circ$  under varying magnetic fields from 0.5 T to 3 T.

11  
12 We numerically demonstrate broadband nonreciprocal emission using a gradient-doped  
13 semiconductor multilayer. To make the ENZ wavelength of doped semiconductor decrease with  
14 the depth, the doping level of the semiconductor is chosen to increase with the depth. As an  
15 example, we consider gradient-doped InSb multilayer, with electron doping levels as  $3.51 \times$   
16  $10^{18} \text{ cm}^{-3}$ ,  $4.21 \times 10^{18} \text{ cm}^{-3}$ ,  $5.15 \times 10^{18} \text{ cm}^{-3}$ ,  $6.36 \times 10^{18} \text{ cm}^{-3}$ , and  $8 \times 10^{18} \text{ cm}^{-3}$ ,  
17 respectively, and with a 400 nm thickness for each layer. In this multilayer, when the permittivity  
18 of a specific layer is near zero, the layer immediately underneath is metallic with relative  
19 permittivity about  $-2$ , corresponding to the thin film case in Fig. 1. The multilayer is backed by a  
20 reflector consisting of 500 nm-thick undoped InSb dielectric spacer layer on top of Au. The spacer  
21 layer is used to enhance the nonreciprocal emission contributed by the bottom doped layer. Figure  
22 3(c) and (d) show the emissivity and absorptivity of the multilayer, respectively, at 3 T magnetic  
23 field. There is strong broadband emission at angle  $\theta > 0$ , corresponding to ENZ wavelengths of  
24 each individual doped layer. In contrast, the absorptivity is negligible for light incident at angle  
25  $\theta > 0$ . Therefore, emissivity exceeds absorptivity over a broad band at  $\theta > 0$ , as shown in Fig.  
26 3(e). In contrast, at angle  $\theta < 0$ , absorptivity exceeds emissivity. Finally, we note substantial  
27 difference between emission and absorption already exists at smaller magnetic fields. Figure 3(f)  
28 shows the difference between emissivity and absorptivity at  $\theta = 50^\circ$  under varying magnetic

1 fields. At  $\theta = 50^\circ$ , the difference between emissivity and absorptivity reaches 0.85 under 3 T  
 2 magnetic field, but is already significant as 0.40 under 1 T magnetic field.

3 Our approach of using gradient ENZ magneto-optical metamaterial for achieving  
 4 broadband nonreciprocal emission is general. In the following, we show another broadband  
 5 nonreciprocal emitter based on magnetic Weyl semimetals (MWS) [53-56]. Magnetic Weyl  
 6 semimetals can break the Lorentz reciprocity without external magnetic field due to strong  
 7 anomalous Hall effect associated with enhanced Berry curvature near Weyl nodes. MWS recently  
 8 have been used to theoretically design nonreciprocal emitters without external magnetic field [36,  
 9 37], though experiments of nonreciprocal emitters based on MWS await to be demonstrated. We  
 10 consider a multilayer emitter which consists of five MWS layers with gradient chemical potential  
 11 on top of Au, as shown in Fig. 4(a). In MWS, the separation  $2b$  between two Weyl nodes in the  
 12 momentum space acts similar to internal magnetization. When the momentum separation of Weyl  
 13 nodes is aligned in  $y$  axis, the relative permittivity tensor of MWS is given by:

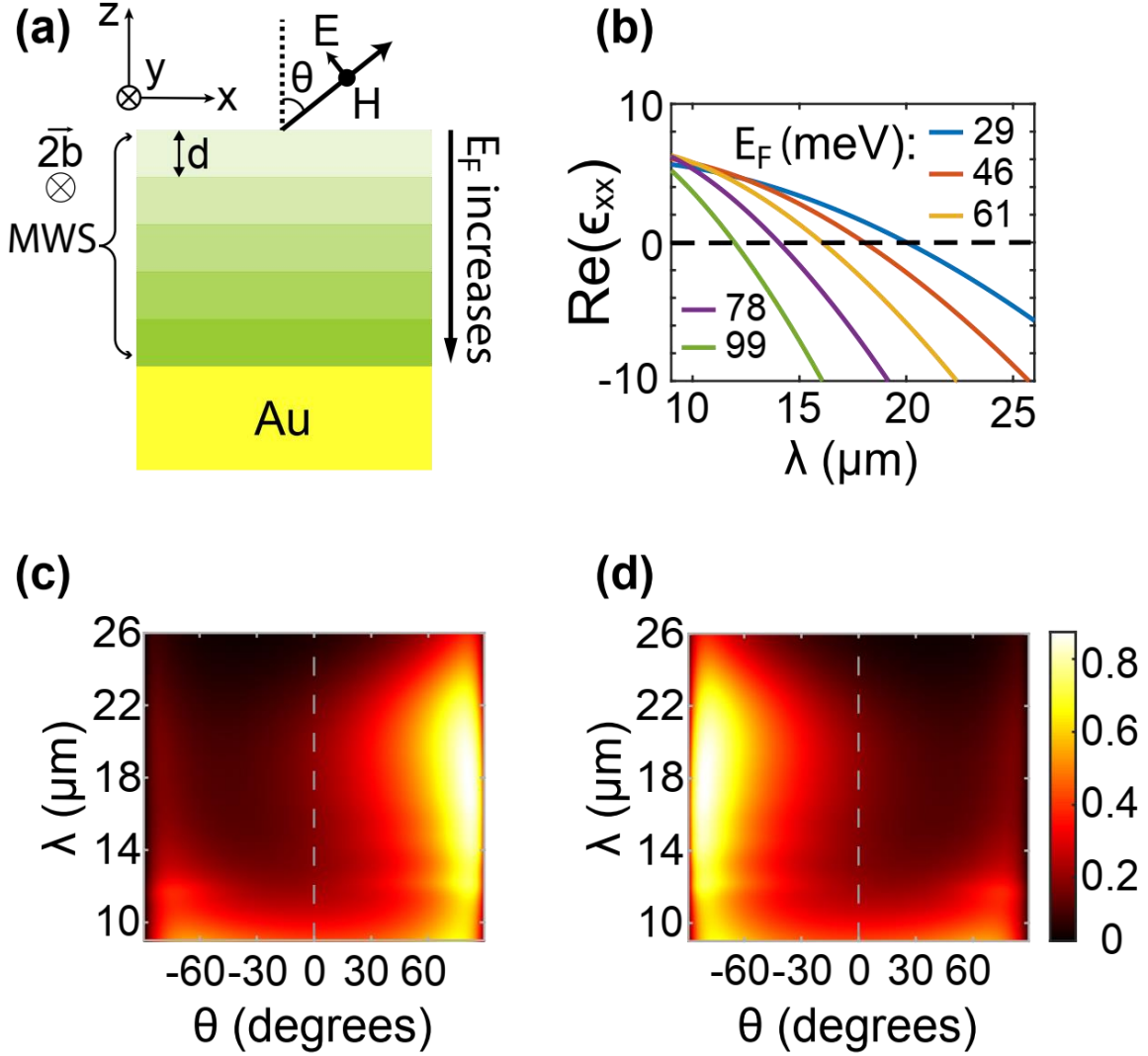
$$14 \quad \vec{\epsilon} = \begin{bmatrix} \epsilon_d & 0 & -i\epsilon_a \\ 0 & \epsilon_d & 0 \\ i\epsilon_a & 0 & \epsilon_d \end{bmatrix},$$

15 where  $\epsilon_a = \frac{be^2}{2\pi^2\hbar\omega}$ . The diagonal term  $\epsilon_d$  has the form:

$$16 \quad \epsilon_d = \epsilon_b - \frac{ir_s g}{6\Omega_0} \Omega G\left(\frac{\Omega}{2}\right) - \frac{r_s g}{6\pi\Omega_0} \left\{ \frac{4}{\Omega} \left[ 1 + \frac{\pi^2}{3} \left( \frac{k_B T}{E_F(T)} \right)^2 \right] + 8\Omega \int_0^{\xi_c} \frac{G(\xi) - G\left(\frac{\Omega}{2}\right)}{\Omega^2 - 4\xi^2} \xi d\xi \right\}.$$

17 We follow Ref. [57] for the dielectric model of MWS. Here,  $\epsilon_b$  is the background permittivity,  
 18  $r_s = \frac{e^2}{4\pi\epsilon_0\hbar v_F}$  is the effective fine-structure constant where  $v_F$  is the Fermi velocity,  $\Omega = \frac{\hbar(\omega+i\tau^{-1})}{E_F}$   
 19 is the normalized complex frequency where  $\tau$  is the scattering time and  $E_F(T)$  is the chemical  
 20 potential as a function of temperature  $T$ ,  $\Omega_0 = \frac{\hbar\omega}{E_F}$  is the normalized real frequency, and  $G(E) =$

1  $n(-E) - n(E)$  where  $n(E) = \frac{1}{e^{\frac{E-E_F}{k_B T}} + 1}$  is the Fermi-Dirac distribution and  $k_B$  is the Boltzmann  
 2 constant. Following Refs. [57, 58], we use  $b = 8.5 \times 10^8 \text{ m}^{-1}$ ,  $\epsilon_b = 6.2$ ,  $v_F = 0.83 \times$   
 3  $10^5 \text{ m s}^{-1}$ ,  $g = 2$ ,  $\xi_c = 3$ , and  $\tau = 450 \text{ fs}$ . With nonzero momentum separation, the permittivity  
 4 tensor of WMS becomes asymmetric, breaking the Lorentz reciprocity. We consider MWS  
 5 multilayer, where each layer has a thickness of 100 nm, and its chemical potential increases with  
 6 depth, as 29 meV, 46 meV, 61 meV, 78 meV, and 99 meV, respectively. As the chemical potential  
 7 increases, the ENZ wavelength shifts to shorter wavelength, as shown in Fig. 4(b).



1 FIG. 4. Broadband nonreciprocal emitter based on magnetic Weyl semimetal (MWS) metamaterial.  
2 (a) Schematic of the emitter consisting of MWS layers with gradient chemical potential atop Au.  
3 Each MWS layer has a thickness of  $100\text{ nm}$ , and its chemical potential increases with depth. (b)  
4 The real part of permittivity tensor component  $\epsilon_{xx}$  as a function of wavelength  $\lambda$  for varying  
5 chemical potentials at  $T = 300\text{ K}$ . (c) Emissivity  $\varepsilon$  and (d) absorptivity  $\alpha$  of the MWS multilayer  
6 with gradient chemical potential.

7  
8 We show the calculated emissivity and absorptivity of the MWS multilayer in Fig. 4 (c-d).

9 The MWS multilayer with gradient chemical potential shows strong broadband emission at  $\theta > 0$ ,  
10 but negligible absorption at the same angles, leading to broadband nonreciprocal emission and  
11 absorption. In contrast, the structure shows negligible emissivity at  $\theta < 0$ , but strong broadband  
12 absorption at the same angles. The achieved spectral bandwidth of nonreciprocal emission is as  
13 large as  $10\text{ }\mu\text{m}$ . The gradient chemical potential for MWS may be achieved experimentally via  
14 doping [59-61] through controlling the types and concentrations of dopants.

15 We compare the broadband nonreciprocal emitters based on semiconductors and those  
16 based on magnetic Weyl semimetals. First, nonreciprocal emitters based on magnetic Weyl  
17 semimetals typically have a broader spectral bandwidth than those based on semiconductors. For  
18 the diagonal element of the relative permittivity, when its real part is near zero, its imaginary part  
19 is  $\sim 0.01$  and  $\sim 1$  for semiconductors and magnetic Weyl semimetals, respectively. As a larger  
20 imaginary part for the permittivity at ENZ wavelength indicates larger intrinsic loss, emitter based  
21 on magnetic Weyl semimetals has broader bandwidth compared with that based on semiconductors.  
22 Second, the angular responses of the two emitters are different. The emitter based magnetic Weyl  
23 semimetals has a narrower angular range than that based on semiconductors. Further, the emission  
24 of broadband nonreciprocal emitter based on magnetic Weyl semimetals peaks at larger angle  
25 compared with that based on semiconductors. Finally, the broadband nonreciprocal emitter based  
26 on semiconductor requires external magnetic field. In contrast, the broadband nonreciprocal  
27 emitter based on magnetic Weyl semimetal is possible to function without external magnetic field.

1     **V. Conclusion and Discussion**

2           In conclusion, we have introduced a general approach to achieve broadband nonreciprocal  
3    emission and absorption by using gradient epsilon-near-zero magneto-optical metamaterial. We  
4    use temporal coupled mode theory to elucidate nonreciprocal emission and absorption in one  
5    magneto-optical layer. We then introduce gradient epsilon-near-zero magneto-optical metamaterial  
6    as a general way for achieving broadband angle-selective nonreciprocal emission and absorption.  
7    We numerically demonstrate broadband nonreciprocal thermal emission in gradient-doped  
8    semiconductor multilayer under magnetic field, as well as in magnetic Weyl semimetal multilayer  
9    with gradient chemical potential without external magnetic field. Our results will be useful for  
10   designing broadband nonreciprocal emitters and absorbers for improving energy conversion, such  
11   as for solar cells, thermophotovoltaics, harvesting outgoing thermal radiation, and for achieving  
12   nonreciprocal radiative thermal management and communication.

13           Finally, we provide a brief discussion on a few aspects towards application of broadband  
14    nonreciprocal emitters including working temperature, operating wavelength, and requirement on  
15    magnetic field. We start by discussing the working temperature of broadband nonreciprocal  
16    emitters. In this work, we considered broadband nonreciprocal emitters at 300 K. First, we  
17    numerically demonstrated broadband nonreciprocal emitters based on InSb, due to its low electron  
18    effective mass, and thus a large cyclotron frequency at a given magnetic field. InSb has a melting  
19    temperature of 800 K. We note that the material choice for achieving broadband nonreciprocal  
20    emission is quite general. Semiconductors [62] such as InAs, InGa<sub>0.47</sub>As<sub>0.53</sub>, GaAs, HgTe, PbTe,  
21    PbSe, and PbS, which have a low effective mass, could be used to achieve similar effects. These  
22    semiconductors have melting temperatures near or higher than 1000 K. Second, certain magnetic  
23    Weyl semimetals have high Curie temperatures, such as Co<sub>2</sub>MnGa at 690 K [53] and Co<sub>2</sub>MnAl at

1 726 K [63]. Thus, broadband nonreciprocal emitters based on semiconductors and Weyl  
2 semimetals have potential to work over a large temperature range. We note as temperature changes,  
3 the optical properties of semiconductors and magnetic Weyl semimetals will change, and thus the  
4 design will need to be modified.

5 We discuss the operating wavelength of broadband nonreciprocal emitters. In our work, as  
6 numerical examples, we demonstrated broadband nonreciprocal emission at wavelengths about  
7 10-20  $\mu\text{m}$ . Depending on the applications, the wavelength range for nonreciprocal emission and  
8 absorption needs be tailored. For solar energy harvesting and thermophotovoltaics, broadband  
9 nonreciprocal emission is required at wavelengths shorter than 10  $\mu\text{m}$ . For harvesting outgoing  
10 radiation from an ambient at 300 K to the outer space, broadband nonreciprocal emission is needed  
11 at the mid infrared. Further, for nonreciprocal heat flux control and communication, the  
12 wavelength range of nonreciprocal emission depends on the temperature of the bodies, and  
13 communication frequency, respectively. The wavelength range can be shifted to shorter (or longer)  
14 wavelengths by increasing (or reducing) the doping concentration of semiconductors, and by  
15 increasing (or reducing) the Fermi level of magnetic Weyl semimetals.

16 We further discuss the requirement for magnetic field for achieving broadband  
17 nonreciprocal emission. For broadband nonreciprocal emitters based on semiconductors, the  
18 difference between emissivity and absorptivity reaches 0.85 under 3  $T$  magnetic field, but is  
19 already significant as 0.40 under 1  $T$  magnetic field. We note that in a recent experiment [64],  
20 magnetic field of similar magnitude (1.2  $T$ ) was generated using ferromagnets to achieve  
21 nonreciprocal absorption. Further, we showed that magnetic Weyl semimetals have potential to  
22 support broadband nonreciprocal emission without using any magnetic field. Thus, our general

1 strategy for achieving broadband nonreciprocal emission will be useful and relevant for  
2 experiments and applications.

3

4 **ACKNOWLEDGMENTS**

5 This work is supported by the Charles E. Kaufman Foundation, a supporting organization of the  
6 Pittsburgh Foundation, and by the start-up funding supported by the Pennsylvania State University.

7

8 **REFERENCES**

- 9 1. S. H. Fan, Thermal Photonics and Energy Applications, *Joule* **1**, 264-273 (2017).
- 10 2. W. Li, and S. H. Fan, Nanophotonic control of thermal radiation for energy applications  
11 [Invited], *Opt. Express* **26**, 15995-16021 (2018).
- 12 3. D. G. Baranov, Y. Z. Xiao, I. A. Nechepurenko, A. Krasnok, A. Alu, and M. A. Kats,  
13 Nanophotonic engineering of far-field thermal emitters, *Nature Materials* **18**, 920-930  
14 (2019).
- 15 4. Y. Li, W. Li, T. C. Han, X. Zheng, J. X. Li, B. W. Li, S. H. Fan, and C. W. Qiu, Transforming  
16 heat transfer with thermal metamaterials and devices, *Nature Reviews Materials* **6**, 488-  
17 507 (2021).
- 18 5. X. L. Liu, T. Tyler, T. Starr, A. F. Starr, N. M. Jokerst, and W. J. Padilla, Taming the  
19 Blackbody with Infrared Metamaterials as Selective Thermal Emitters, *Phys. Rev. Lett.* **107**,  
20 045901 (2011).
- 21 6. P. N. Dyachenko, S. Molesky, A. Y. Petrov, M. Stormer, T. Krekeler, S. Lang, M. Ritter, Z.  
22 Jacob, and M. Eich, Controlling thermal emission with refractory epsilon-near-zero  
23 metamaterials via topological transitions, *Nature Communications* **7**, 11809 (2016).
- 24 7. M. Zhou, E. Khoram, D. J. Liu, B. Y. Liu, S. H. Fan, M. L. Povinelli, and Z. F. Yu, Self-  
25 Focused Thermal Emission and Holography Realized by Mesoscopic Thermal Emitters,  
26 *ACS Photonics* **8**, 497-504 (2021).
- 27 8. A. C. Overvig, S. A. Mann, and A. Alu, Thermal Metasurfaces: Complete Emission Control  
28 by Combining Local and Nonlocal Light-Matter Interactions, *Physical Review X* **11**,  
29 021050 (2021).
- 30 9. S. Y. Lin, J. G. Fleming, D. L. Hetherington, B. K. Smith, R. Biswas, K. M. Ho, M. M.  
31 Sigalas, W. Zubrzycki, S. R. Kurtz, and J. Bur, A three-dimensional photonic crystal  
32 operating at infrared wavelengths, *Nature* **394**, 251-253 (1998).
- 33 10. D. L. C. Chan, M. Soljačić, and J. D. Joannopoulos, Thermal emission and design in 2D-  
34 periodic metallic photonic crystal slabs, *Opt. Express* **14**, 8785-8796 (2006).
- 35 11. T. Inoue, M. De Zoysa, T. Asano, and S. Noda, Realization of dynamic thermal emission  
36 control, *Nature Materials* **13**, 928-931 (2014).
- 37 12. A. P. Raman, M. A. Anoma, L. Zhu, E. Rephaeli, and S. Fan, Passive radiative cooling  
38 below ambient air temperature under direct sunlight, *Nature* **515**, 540-544 (2014).

1 13. J. Xu, J. Mandal, and A. P. Raman, Broadband directional control of thermal emission,  
2 *Science* **372**, 393-397 (2021).

3 14. S. Vassant, J. P. Hugonin, F. Marquier, and J. J. Greffet, Berreman mode and epsilon near  
4 zero mode, *Opt. Express* **20**, 23971-23977 (2012).

5 15. I. Liberal, and N. Engheta, Manipulating thermal emission with spatially static fluctuating  
6 fields in arbitrarily shaped epsilon-near-zero bodies, *Proceedings of the National Academy  
7 of Sciences* **115**, 2878-2883 (2018).

8 16. V. W. Brar, M. C. Sherrott, M. S. Jang, S. Kim, L. Kim, M. Choi, L. A. Sweatlock, and H.  
9 A. Atwater, Electronic modulation of infrared radiation in graphene plasmonic resonators,  
10 *Nature Communications* **6**, 7032 (2015).

11 17. R.-J. Shiue, Y. Gao, C. Tan, C. Peng, J. Zheng, D. K. Efetov, Y. D. Kim, J. Hone, and D.  
12 Englund, Thermal radiation control from hot graphene electrons coupled to a photonic  
13 crystal nanocavity, *Nature Communications* **10**, 109 (2019).

14 18. M. A. Kats, R. Blanchard, S. Y. Zhang, P. Genevet, C. H. Ko, S. Ramanathan, and F.  
15 Capasso, Vanadium Dioxide as a Natural Disordered Metamaterial: Perfect Thermal  
16 Emission and Large Broadband Negative Differential Thermal Emittance, *Physical Review  
17 X* **3**, 041004 (2013).

18 19. A. Lenert, D. M. Bierman, Y. Nam, W. R. Chan, I. Celanovic, M. Soljacic, and E. N. Wang,  
19 A nanophotonic solar thermophovoltaic device, *Nat. Nanotechnol.* **9**, 126-130 (2014).

20 20. Z. Omair, G. Scranton, L. M. Pazos-Outón, T. P. Xiao, M. A. Steiner, V. Ganapati, P. F.  
21 Peterson, J. Holzrichter, H. Atwater, and E. Yablonovitch, Ultraefficient  
22 thermophovoltaic power conversion by band-edge spectral filtering, *Proceedings of the  
23 National Academy of Sciences* **116**, 15356-15361 (2019).

24 21. D. J. Fan, T. Burger, S. McSherry, B. Lee, A. Lenert, and S. R. Forrest, Near-perfect photon  
25 utilization in an air-bridge thermophovoltaic cell, *Nature* **586**, 237-241 (2020).

26 22. M. L. Brongersma, Y. Cui, and S. Fan, Light management for photovoltaics using high-  
27 index nanostructures, *Nature Materials* **13**, 451-460 (2014).

28 23. Z. Yu, A. Raman, and S. Fan, Fundamental limit of nanophotonic light trapping in solar  
29 cells, *Proceedings of the National Academy of Sciences* **107**, 17491-17496 (2010).

30 24. Y. Zhai, Y. G. Ma, S. N. David, D. L. Zhao, R. N. Lou, G. Tan, R. G. Yang, and X. B. Yin,  
31 Scalable-manufactured randomized glass-polymer hybrid metamaterial for daytime  
32 radiative cooling, *Science* **355**, 1062-1066 (2017).

33 25. G. Kirchhoff, Ueber das Verhältniss zwischen dem Emissionsvermögen und dem  
34 Absorptionsvermögen der Körper für Wärme und Licht, *Annalen der Physik* **185**, 275-301  
35 (1860).

36 26. M. Planck, *The Theory of Heat Radiation*. (Dover Publications, 2013).

37 27. R. Siegel, *Thermal Radiation Heat Transfer, Fourth Edition*. (Taylor & Francis, 2001).

38 28. H. Ries, Complete and reversible absorption of radiation, *Applied Physics B* **32**, 153-156  
39 (1983).

40 29. M. A. Green, Time-Asymmetric Photovoltaics, *Nano Lett.* **12**, 5985-5988 (2012).

41 30. Y. B. Park, B. Zhao, and S. H. Fan, Reaching the Ultimate Efficiency of Solar Energy  
42 Harvesting with a Nonreciprocal Multijunction Solar Cell, *Nano Lett.* **22**, 448-452 (2022).

43 31. S. Buddhiraju, P. Santhanam, and S. H. Fan, Thermodynamic limits of energy harvesting  
44 from outgoing thermal radiation, *Proc. Natl. Acad. Sci. U. S. A.* **115**, E3609-E3615 (2018).

45 32. W. Li, S. Buddhiraju, and S. Fan, Thermodynamic limits for simultaneous energy  
46 harvesting from the hot sun and cold outer space, *Light: Science & Applications* **9**, 68

1 (2020).

2 33. Z. Zhang, and L. Zhu, Nonreciprocal thermal photonics for energy conversion and radiative  
3 heat transfer, *Physical Review Applied* **18**, 027001 (2022).

4 34. Y. Hadad, J. C. Soric, and A. Alu, Breaking temporal symmetries for emission and  
5 absorption, *Proc. Natl. Acad. Sci. U. S. A.* **113**, 3471-3475 (2016).

6 35. L. Zhu, and S. Fan, Near-complete violation of detailed balance in thermal radiation,  
7 *Physical Review B* **90**, 220301(R) (2014).

8 36. B. Zhao, C. Guo, C. A. C. Garcia, P. Narang, and S. H. Fan, Axion-Field-Enabled  
9 Nonreciprocal Thermal Radiation in Weyl Semimetals, *Nano Lett.* **20**, 1923-1927 (2020).

10 37. Y. Tsurimaki, X. Qian, S. Pajovic, F. Han, M. D. Li, and G. Chen, Large nonreciprocal  
11 absorption and emission of radiation in type-I Weyl semimetals with time reversal  
12 symmetry breaking, *Physical Review B* **101**, 165426 (2020).

13 38. Z. M. Zhang, X. H. Wu, and C. J. Fu, Validity of Kirchhoff's law for semitransparent films  
14 made of anisotropic materials, *Journal of Quantitative Spectroscopy & Radiative Transfer*  
15 **245**, 106904 (2020).

16 39. C. Khandekar, R. Messina, and A. W. Rodriguez, Near-field refrigeration and tunable heat  
17 exchange through four-wave mixing, *AIP Advances* **8**, 055029 (2018).

18 40. S. Buddhiraju, W. Li, and S. H. Fan, Photonic Refrigeration from Time-Modulated Thermal  
19 Emission, *Phys. Rev. Lett.* **124**, 077402 (2020).

20 41. J. Wu, F. Wu, and X. H. Wu, Strong dual-band nonreciprocal radiation based on a four-part  
21 periodic metal grating, *Optical Materials* **120**, 111476 (2021).

22 42. J. Wu, F. Wu, T. C. Zhao, M. Antezza, and X. H. Wu, Dual-band nonreciprocal thermal  
23 radiation by coupling optical Tamm states in magnetophotonic multilayers, *Int. J. Therm.  
24 Sci.* **175**, 107457 (2022).

25 43. K. Seeger, *Semiconductor Physics : An Introduction*. Advanced Texts in Physics (Springer,  
26 Berlin, Heidelberg, ed. 9, 2004).

27 44. E. Litwin-Staszewska, W. Szymańska, and R. Piotrzkowski, The Electron Mobility and  
28 Thermoelectric Power in InSb at Atmospheric and Hydrostatic Pressures, *physica status  
29 solidi (b)* **106**, 551-559 (1981).

30 45. P. Byszewski, J. Kołodziejczak, and S. Zukotyński, The Thermoelectric Power in InSb in  
31 the Presence of an External Magnetic Field, *physica status solidi (b)* **3**, 1880-1884 (1963).

32 46. S. Law, R. Liu, and D. Wasserman, Doped semiconductors with band-edge plasma  
33 frequencies, *Journal of Vacuum Science & Technology B* **32**, 052601 (2014).

34 47. S. Rytov, Y. A. Kravtsov, and V. Tatarskii, *Principles of Statistical Radiophysics*. (Springer,  
35 Berlin, 1989).

36 48. D. Polder, and M. Vanhove, THEORY OF RADIATIVE HEAT TRANSFER BETWEEN  
37 CLOSELY SPACED BODIES, *Physical Review B* **4**, 3303 (1971).

38 49. L. X. Zhu, S. Sandhu, C. Otey, S. H. Fan, M. B. Sinclair, and T. S. Luk, Temporal coupled  
39 mode theory for thermal emission from a single thermal emitter supporting either a single  
40 mode or an orthogonal set of modes, *Appl. Phys. Lett.* **102**, 103104 (2013).

41 50. See Supplemental Material at [URL will be inserted by publisher] for derivation of  
42 dispersion relation of thin film emitter.

43 51. A. Raman, W. Shin, and S. Fan, Upper Bound on the Modal Material Loss Rate in  
44 Plasmonic and Metamaterial Systems, *Phys. Rev. Lett.* **110**, 183901 (2013).

45 52. C. Guo, B. Zhao, and S. Fan, Adjoint Kirchhoff's Law and General Symmetry Implications  
46 for All Thermal Emitters, *Physical Review X* **12**, 021023 (2022).

1 53. I. Belopolski, K. Manna, D. S. Sanchez, G. Q. Chang, B. Ernst, J. X. Yin, S. S. Zhang, T.  
2 Cochran, N. Shumiya, H. Zheng, B. Singh, G. Bian, D. Multer, M. Litskevich, X. T. Zhou,  
3 S. M. Huang, B. K. Wang, T. R. Chang, S. Y. Xu, A. Bansil, C. Felser, H. Lin, and M. Z.  
4 Hasan, Discovery of topological Weyl fermion lines and drumhead surface states in a room  
5 temperature magnet, *Science* **365**, 1278-1281 (2019).

6 54. D. F. Liu, A. J. Liang, E. K. Liu, Q. N. Xu, Y. W. Li, C. Chen, D. Pei, W. J. Shi, S. K. Mo,  
7 P. Dudin, T. Kim, C. Cacho, G. Li, Y. Sun, L. X. Yang, Z. K. Liu, S. S. P. Parkin, C. Felser,  
8 and Y. L. Chen, Magnetic Weyl semimetal phase in a Kagome crystal, *Science* **365**, 1282-  
9 1285 (2019).

10 55. N. Morali, R. Batabyal, P. K. Nag, E. K. Liu, Q. A. Xu, Y. Sun, B. H. Yan, C. Felser, N.  
11 Avraham, and H. Beidenkopf, Fermi-arc diversity on surface terminations of the magnetic  
12 Weyl semimetal Co<sub>3</sub>Sn<sub>2</sub>S<sub>2</sub>, *Science* **365**, 1286-1291 (2019).

13 56. P. G. Li, J. Koo, W. Ning, J. G. Li, L. X. Miao, L. J. Min, Y. L. Zhu, Y. Wang, N. Alem, C.  
14 X. Liu, Z. Q. Mao, and B. H. Yan, Giant room temperature anomalous Hall effect and  
15 tunable topology in a ferromagnetic topological semimetal Co<sub>2</sub>MnAl, *Nature  
16 Communications* **11**, 3476 (2020).

17 57. C. Guo, B. Zhao, D. H. Huang, and S. H. Fan, Radiative Thermal Router Based on Tunable  
18 Magnetic Weyl Semimetals, *ACS Photonics* **7**, 3257-3263 (2020).

19 58. O. V. Kotov, and Y. E. Lozovik, Giant tunable nonreciprocity of light in Weyl semimetals,  
20 *Physical Review B* **98**, 195446 (2018).

21 59. K. Halterman, M. Alidoust, and A. Zyuzin, Epsilon-near-zero response and tunable perfect  
22 absorption in Weyl semimetals, *Physical Review B* **98**, 085109 (2018).

23 60. E. Haubold, K. Koepernik, D. Efremov, S. Khim, A. Fedorov, Y. Kushnirenko, J. van den  
24 Brink, S. Wurmehl, B. Buchner, T. K. Kim, M. Hoesch, K. Sumida, K. Taguchi, T.  
25 Yoshikawa, A. Kimura, T. Okuda, and S. V. Borisenko, Experimental realization of type-II  
26 Weyl state in noncentrosymmetric TaIrTe<sub>4</sub>, *Physical Review B* **95**, 241108(R) (2017).

27 61. M. Chinotti, A. Pal, W. J. Ren, C. Petrovic, and L. Degiorgi, Electrodynamic response of  
28 the type-II Weyl semimetal YbMnBi<sub>2</sub>, *Physical Review B* **94**, 245101 (2016).

29 62. O. Madelung, *Semiconductors: Data Handbook*. (Springer, Berlin, ed. 3rd, 2004).

30 63. R. Y. Umetsu, K. Kobayashi, A. Fujita, R. Kainuma, and K. Ishida, Magnetic properties  
31 and stability of L2(1) and B2 phases in the Co<sub>2</sub>MnAl Heusler alloy, *J. Appl. Phys.* **103**,  
32 07D718 (2008).

33 64. K. J. Shayegan, B. Zhao, Y. Kim, S. H. Fan, and H. A. Atwater, Nonreciprocal infrared  
34 absorption via resonant magneto-optical coupling to InAs, *Science Advances* **8**, eabm4308  
35 (2022).

36